# SKEL-CF: Coarse-to-Fine Biomechanical Skeleton and Surface Mesh Recovery

Da Li<sup>1,2\*</sup>, Ji-Ping Jin<sup>1,3\*</sup>, Xuanlong Yu<sup>1</sup>, Wei Liu<sup>5</sup>, Xiaodong Cun<sup>4</sup>, Kai Chen<sup>5</sup>, Rui Fan<sup>3</sup>, Jiangang Kong<sup>5</sup>, Xi Shen<sup>1,†</sup>

\*Equal contribution †Co

†Corresponding author

<sup>1</sup>Intellindust AI Lab <sup>2</sup>Shenzhen University <sup>3</sup>ShanghaiTech University <sup>4</sup>Great Bay University <sup>5</sup>Didi Chuxing Co.Ltd

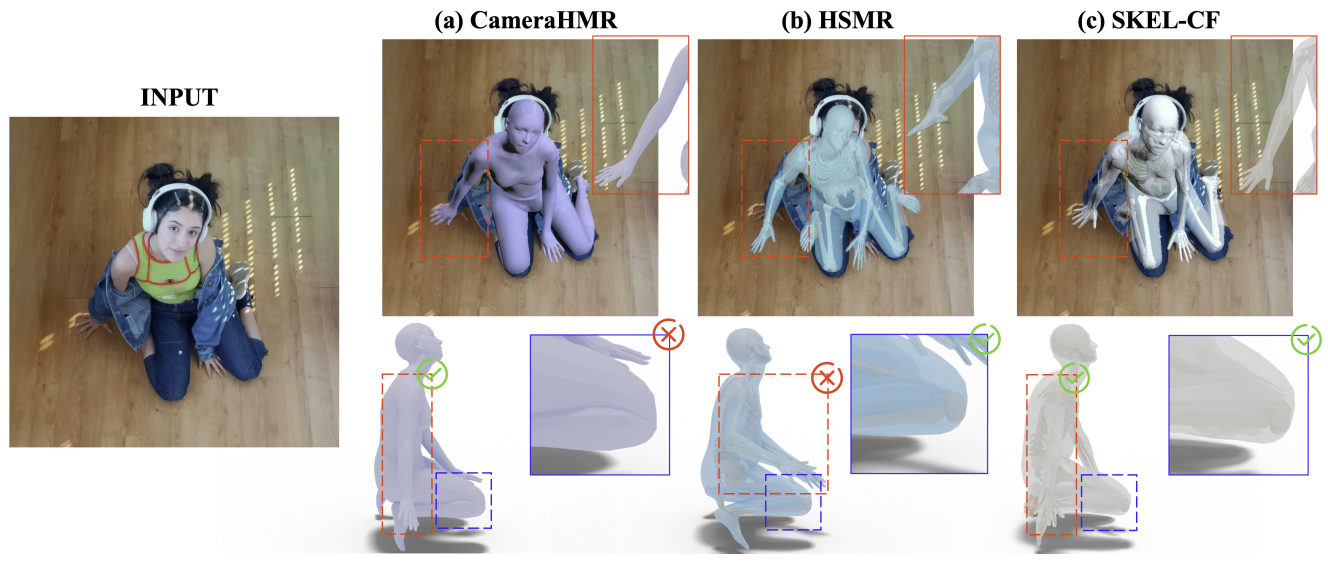


Figure 1. **Visualization of SKEL-CF on web images.** Compared with SMPL-based state-or-the-art CameraHMR [27], our SKEL-based model produces more natural joint motions (see the side-view zoomed knee in blue). Compared with HSMR [39], the state-of-the-art SKEL-based method, SKEL-CF achieves more accurate skeleton and mesh reconstruction (see zoomed hand in orange).

#### **Abstract**

Parametric 3D human models such as SMPL have driven significant advances in human pose and shape estimation, yet their simplified kinematics limit biomechanical realism. The recently proposed SKEL model addresses this limitation by re-rigging SMPL with an anatomically accurate skeleton. However, estimating SKEL parameters directly remains challenging due to limited training data, perspective ambiguities, and the inherent complexity of human articulation. We introduce SKEL-CF, a coarse-to-fine framework for SKEL parameter estimation. SKEL-CF employs a transformer-based encoder-decoder architecture, where the encoder predicts coarse camera and SKEL parameters, and the decoder progressively refines them in successive layers. To ensure anatomically consistent supervision, we convert the existing SMPL-based dataset 4DHuman into a SKEL-aligned version, 4DHuman-SKEL, providing high-quality training data for SKEL estimation. In addition, to mitigate depth and scale ambiguities, we explicitly incorporate camera modeling into the SKEL-CF pipeline and demonstrate its importance across diverse viewpoints. Extensive experiments validate the effectiveness of the proposed design. On the challenging MOYO dataset, SKEL-CF achieves 85.0 MPJPE / 51.4 PA-MPJPE, significantly outperforming the previous SKEL-based state-of-theart HSMR (104.5 / 79.6). These results establish SKEL-CF as a scalable and anatomically faithful framework for human motion analysis, bridging the gap between computer vision and biomechanics. Our implementation is available on the project page: https://pokerman8.github.io/SKEL-CF/.

#### 1. Introduction

In recent years, 3D human pose and shape estimation has made remarkable progress, enabling a wide range of downstream applications [5, 8, 19, 32, 37]. However, adoption in biomechanics, a domain where such techniques could be particularly impactful, remains limited. This gap arises because existing parametric models, such as SMPL [23], SMPL-X [28], and GHUM [40], fall short of the stringent biomechanical requirements. Their simplified kinematics and loosely constrained axis—angle representations often compromise biomechanical realism, especially in complex articulations such as deep squats or yoga poses [39]. In these scenarios, the estimated parameters must correspond to anatomically accurate skeletons, respect joint limits, and ensure physically plausible motion with high precision. As illustrated in Figure 1 (a), even the state-of-the-art SMPL-based method CameraHMR [27] can produce anatomically implausible results, such as unnatural knee bending.

To address these limitations, the recently proposed SKEL [15] model redefines the foundation of human representation by re-rigging SMPL with an anatomically accurate skeleton and realistic joint constraints. This makes it a promising step toward bridging computer vision and biomechanics, offering a representation that is both visually coherent and biomechanically faithful. HSMR [39] is the first transformer-based method to reconstruct a human body in the SKEL space from a single image. It converts the predicted SMPL ground truth from existing datasets into SKEL pseudo ground truth for supervised training. However, estimating SKEL from a single image remains challenging, as it requires inferring 3D structure from inherently limited 2D observations. Consequently, the predictions often lack accuracy (see Figure 1 (b)), and empirical metrics such as MPJPE remain inferior to SMPL-based models.

In this work, we take a step forward in advancing SKELbased human mesh recovery. We observe that estimating SKEL parameters in a coarse-to-fine manner significantly improves performance. Specifically, our transformer encoder first predicts coarse camera and SKEL parameters, while the decoder refines these estimates progressively, layer by layer, leading to more accurate and stable results. To address challenges arising from diverse camera viewpoints, we incorporate camera intrinsic estimation following CameraHMR [27], which enhances the robustness of the reconstructed mesh across varying perspectives. Moreover, by leveraging the high-quality SMPL estimations provided by the recent 4DHuman dataset, we generate large-scale, high-fidelity SKEL annotations to form the 4DHuman-SKEL dataset, enabling more reliable training for SKEL estimation.

Empirically, our proposed SKEL-CF achieves substantial performance gains across diverse benchmarks. On the challenging MOYO dataset [33], SKEL-CF reaches 85.0 MPJPE and 51.4 PA-MPJPE, significantly outperforming the previous SKEL-based state-of-the-art HSMR [39], which reports 104.5 and 79.6, respectively. Further-

more, SKEL-CF attains comparable or superior quantitative performance to leading SMPL-based approaches such as CameraHMR [27] across multiple datasets, including 3DPW [35], EMDB [14], and MOYO [33], while producing biomechanically faithful and visually consistent mesh reconstructions (See igure 1 (c)) These results position SKEL-CF as a robust and anatomically realistic solution for practical human mesh recovery in real-world scenarios. We also conduct ablation studies to validate the contribution of each proposed component in our framework.

To conclude, our key contributions are summarized as follows:

- We propose SKEL-CF, a coarse-to-fine transformer framework that significantly advances SKEL-based human mesh recovery. By explicitly modeling the camera and refining SKEL parameters layer by layer, SKEL-CF achieves state-of-the-art performance across multiple benchmarks while maintaining biomechanical fidelity.
- We demonstrate that estimating SKEL parameters in a coarse-to-fine and iterative refinement manner leads to substantial performance gains. The decoder progressively improves predictions across layers, effectively handling complex articulations and challenging poses.
- We introduce 4DHuman-SKEL, a large-scale, highquality dataset with anatomically consistent SKEL annotations converted from 4DHuman [6]. This dataset provides reliable supervision and unified skeleton-mesh alignment, enabling robust SKEL-based model training.

Our implementation is available on the project page: https://pokerman8.github.io/SKEL-CF/.

## 2. Related Work

Parametric human body model. Parametric human body models are widely used for 3D human shape and pose estimation, as they offer a structured low-dimensional representation of human geometry. SMPL [23] represents the human mesh with fixed topology, using lowdimensional shape and pose parameters with linear blend skinning and pose-dependent corrective shapes for realistic articulation. SMPL-H [29] augments this framework with articulated hands, while SMPL-X [28] further integrates the FLAME [20] facial model, yielding a unified representation of body, hands, and expressive face. while the SMPL family provides a compact and effective representation of the human body surface, it employs a simplified kinematic strcture that deviates from the anatomical skeletal system of real humans, thereby producing unnatural poses. SKEL [15] addresses this limitation by introducing anatomically accurate joint definitions and bone hierarchies, enabling more faithful modeling of human articulation. Moreover, it can generate an internal skeletal mesh aligned with the outer body surface, facilitating applications that require explicit

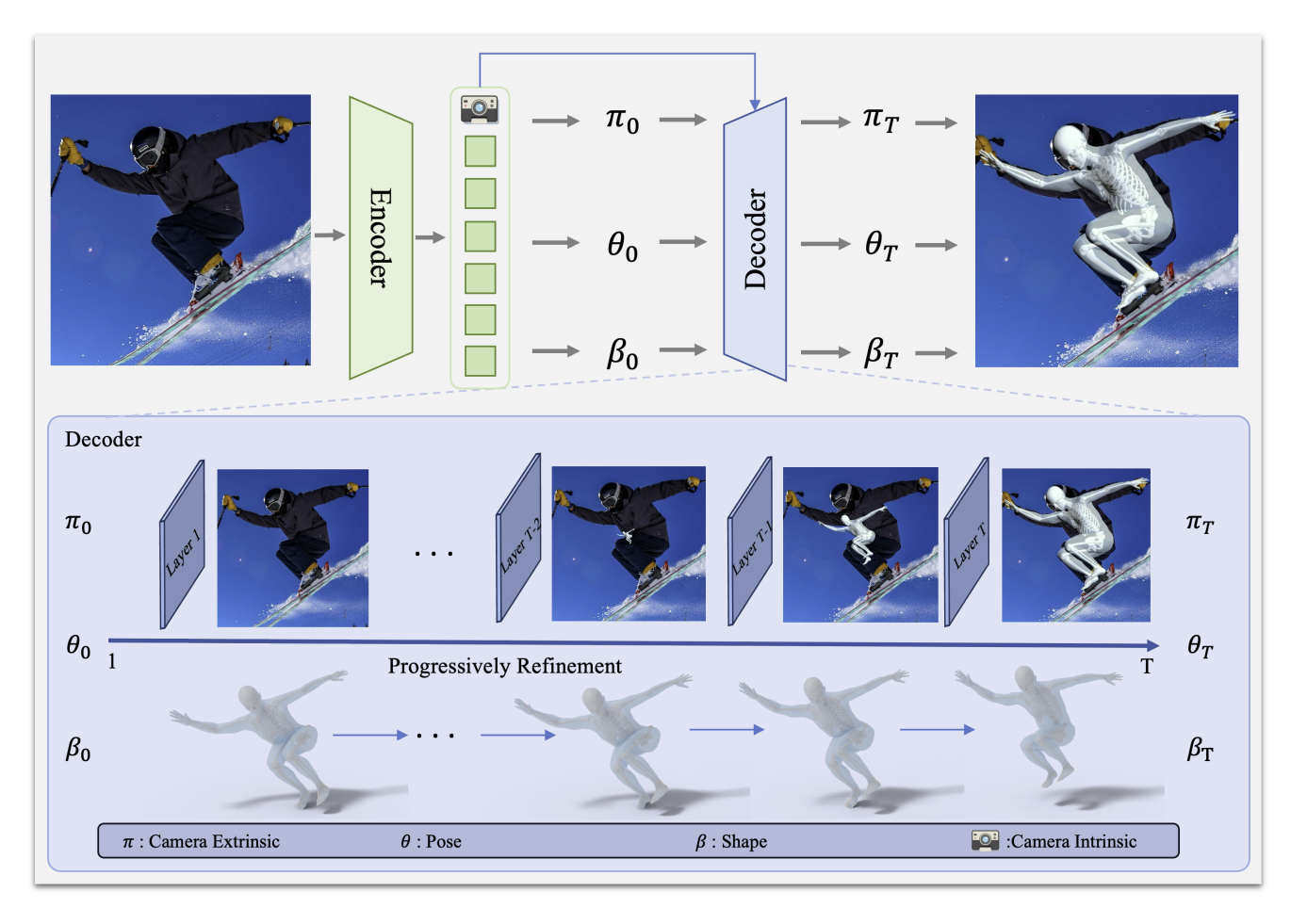


Figure 2. Overview of the proposed SKEL-CF. Our method estimates SKEL parameters from a single image using an encoder–decoder architecture that performs coarse-to-fine estimation. The encoder produces initial predictions of the camera extrinsics  $\pi$ , shape parameters  $\beta$ , and pose parameters  $\theta$ . The decoder then refines these predictions progressively across layers. In addition, we adopt the camera model from CameraHMR [27] to estimate the camera intrinsics.

bone geometry, such as biomechanics analysis, physicsbased simulation, and human-object interaction.

Human mesh recovery. The lack of 3D annotations for in-the-wild images remains a major obstacle in Human mesh recovery. SMPLify [2] mitigates this by iteratively optimizing SMPL [23] parameters from 2D keypoints, yielding accurate results but at high computational cost. HMR [11] introduces the first end-to-end framework to predict 3D pose and shape from in-the-wild images using only 2D supervision, where adversarial learning with mocap data provides strong pose and shape priors to compensate for the missing 3D information. 4DHuman [6] constructs a large-scale dataset by fitting approximately 300 million images with ProHMR [18], generating pseudo-ground-truth (p-GT) 3D annotations alongside 2D keypoints, and further upgrades the network architecture from CNN to Vision Transformer (ViT). However, TokenHMR [4] identi-

fies a mismatch between 3D and 2D keypoints, where enforcing 2D keypoint alignment can degrade 3D evaluation metrics, partly due to the use of fixed camera intrinsics and p-GT annotations in the 4DHuman [6] dataset. To address this, TokenHMR [4] introduces the TALS loss, which down-weights the 2D keypoint loss when the L2 distance between predicted and ground-truth keypoints falls within a predefined threshold, thus preventing overfitting to noisy p-GT annotations. In addition, it leverages a quantized token dictionary, constructed by pre-training a Vector Quantized-VAE (VO-VAE) [34] on motion capture datasets [25, 33], to mitigate 3D pose ambiguity. CameraHMR [27] improves the 4DHuman [6] dataset through CamSMPLify, which refines body representations using dense keypoints to overcome the 'average body' limitation. To tackle the fixedcamera constraint, it introduces HumanFOV [27], transforming weak-perspective projection into a fully perspective projection. Also, by employing the CLIFF [21] method,

CameraHMR [27] enriches global full-frame features with local location information. While most prior efforts focus on SMPL parameter regression, its limited skeletal fidelity motivates a shift toward models with more anatomically accurate joint definitions and internal skeleton representations, namely SKEL [15]. HSMR [39] presents the first end-to-end framework for SKEL parameter regression by fitting SMPL [23] parameters from the 4DHuman dataset to their SKEL counterparts. Given the inherent inaccuracies and artifacts in these pseudo-labels, HSMR introduces Skelify [39], an iterative refinement strategy that progressively improves the training annotations during optimization.

SMPL-to-SKEL dataset conversion. The first largescale 3D pseudo-ground-truth (p-GT) dataset was introduced by 4DHuman [6], which extends to unlabeled datasets such as InstaVariety [13], AVA [7], and AI Challenger [31] by generating p-GT annotations. For each image, an off-the-shelf detector [3] and a body keypoint estimator are applied to obtain bounding boxes and 2D keypoints. A SMPL [23] mesh is then fitted to these keypoints using ProHMR [18], producing pseudo-ground-truth SMPL parameters. Despite its scale and utility, the 4DHuman dataset still contains inaccuracies and artifacts. To that end, CameraHMR [27] refines the dataset using its proposed CamSMPLify method, alongside additional techniques to enhance annotation quality. While large-scale datasets of SMPL parameters have been constructed, there remains a need to develop datasets for SKEL [15] parameters. HSMR [39] addresses this by first converting the 4DHuman SMPL parameters to SKEL parameters using SKEL fitting [15]. To mitigate the inaccuracies in 4DHuman annotations, we further apply SKEL fitting to the refined SMPL annotations provided by CameraHMR.

#### 3. Method

In this section, we introduce our approach, SKEL-CF, whose overall pipeline is illustrated in Figure 2. SKEL-CF aims to estimate SKEL parameters from a single image using an encoder–decoder architecture that performs coarse-to-fine estimation. The encoder produces initial predictions of the camera extrinsics  $\pi_0$ , shape parameters  $\beta_0$ , and pose parameters  $\theta_0$ , while the decoder progressively refines these predictions across layers. To enhance robustness to camera variations, we adopt the camera model from CameraHMR [27] for estimating the camera intrinsics.

This section is organized as follows. We first introduce the SKEL model and the 4DHuman-SKEL dataset that we construct to supervise SKEL learning in Section 3.1. We then describe the details of SKEL-CF and its implementation in Section 3.2.

#### 3.1. Preliminaries

**SKEL model.** The SKEL model [15] is a parametric representation of the human body that enables the joint reconstruction of both the skin surface and the skeletal mesh. Given the pose parameters  $q \in \mathbb{R}^{46}$  and the shape parameters  $\beta \in \mathbb{R}^{10}$  (corresponding to the top 10 shape components), SKEL generates the human mesh  $M \in \mathbb{R}^{6890 \times 3}$  and the skeleton mesh  $S_k \in \mathbb{R}^{24752 \times 3}$ . Unlike SMPL, which defines pose parameters  $\theta \in \mathbb{R}^{72}$  using unrestricted three-degree-of-freedom ball joints, SKEL constrains the motion of each joint, reducing the parameter space from 72 to 46. This formulation ensures anatomically consistent and biomechanically valid poses [15, 39]. Consequently, SKEL produces physically plausible human motion and is particularly suitable for downstream applications such as motion analysis, rehabilitation, and human-robot interaction.

**4DHuman-SKEL:** a high-quality dataset for SKEL training. HSMR [39] initially generated pseudo ground-truth (p-GT) SKEL parameters by fitting the 4DHuman SMPL [23] annotations into the SKEL [15] parameter space. While this conversion provided a practical starting point, its quality was limited by the low-resolution images and noisy annotations in the original 4DHuman [6] dataset, which aggregates samples from Human3.6M [9], MPI-INF-3DHP [26], COCO [22], MPII [1], AI Challenger [38], AVA [7] and InstaVariety [12]. With the recent release of the refined 4DHuman dataset [6] from CameraHMR [27], we revisit this process to obtain higher-quality SKEL p-GT annotations.

Specifically, we first reconstruct the human mesh from the provided SMPL [23] parameters using the neutral SMPL model. While our overall procedure follows the SKEL [15] fitting protocol, we adapt it to better align with the refined 4DHuman dataset [6]. Starting from an initial set of SKEL parameters (shape  $\beta$ , pose  $\theta$ , and camera extrinsics  $\pi$ ), we iteratively optimize the SKEL mesh to match the reconstructed SMPL mesh. Since both models share identical global orientation and translation, we directly convert the SMPL global orientation from axis-angle to Euler angles to comply with the SKEL convention and fix these parameters during optimization. We observe that further optimizing or re-learning global orientation and translation does not improve alignment quality on the refined dataset. The remaining body parts are optimized in a hierarchical manner, first refining upper-limb poses, then optimizing the full-body pose with a fixed root, and finally performing unconstrained fine-tuning for precise mesh alignment.

#### 3.2. SKEL-CF

**Overall pipeline.** As illustrated in Figure 2, SKEL-CF employs an encoder–decoder architecture with a coarse-to-fine strategy to estimate SKEL parameters from a sin-

Methods	3DPV	V [35]	Human3	.6M [9]	MOYO [33]		
	MPJPE ↓	PA-MPJPE↓	MPJPE↓	PA-MPJPE↓	MPJPE↓	PA-MPJPE↓	
HMR2.0 + SKEL fit [15, 39]*	81.0	54.4	53.6	34.1	130.5	93.7	
HSMR [39]	81.5	54.8	50.4	32.9	104.5	79.6	
SKEL-CF (Ours)	<b>61.5</b> (†24.5%)	<b>38.7</b> (†29.3%)	<b>39.0</b> (†22.6%)	<b>31.2</b> (†5.4%)	<b>85.0</b> (†18.6%)	<b>51.4</b> (†35.4%)	

Table 1. Quantitative comparison of skeleton and surface mesh recovery using the SKEL [15] human model on 3DPW [35], Human3.6M [9], and MOYO [33]. The proposed SKEL-CF delivers consistent accuracy gains over previous approaches, with relative improvements shown in green. \* denotes results reported by [39].

gle RGB image. We denote the target parameter set as  $\Theta = \{\theta, \beta, \pi\}$ , where  $\theta$  represents the human pose,  $\beta$  the body shape, and  $\pi$  the camera extrinsics.

Given an input image, the encoder first divides it into visual tokens and, together with camera intrinsic information, extracts contextual features through standard self-attention. Using these features, the encoder produces initial estimates  $\Theta_0 = \{\theta_0, \beta_0, \pi_0\}$ . These initial predictions are then progressively refined through T decoder layers using crossattention with the encoded visual features as context. The final output of SKEL-CF is  $\Theta_T = \{\theta_T, \beta_T, \pi_T\}$ .

Given the pose  $\boldsymbol{\theta}$  and shape  $\boldsymbol{\beta}$ , the corresponding K 3D joint positions  $\mathbf{J}_{3d} \in \mathbb{R}^{K \times 3}$  can be reconstructed via the forward kinematics function. These 3D joints are then projected onto the full image plane using the camera parameters to obtain 2D joint locations  $\mathbf{J}_{2d} \in \mathbb{R}^{K \times 2}$ . The resulting 2D joints provide pixel-level supervision, ensuring consistency between the 3D reconstruction and the image evidence. The training supervision includes the pseudoground-truth pose  $\hat{\boldsymbol{\theta}}$ , shape  $\hat{\boldsymbol{\beta}}$ , 3D joints derived from the pose and shape  $\hat{\mathbf{J}}_{3d}$ , and 2D keypoint annotations  $\hat{\mathbf{J}}_{2d}$ . Note that no direct camera supervision  $\hat{\boldsymbol{\pi}}$  is provided, the camera parameters are learned solely from 2D keypoint supervision, making the training challenging and weakly supervised.

**Learning objectives.** To learn SKEL parameters effectively, we apply multiple supervision signals for accurate 3D human reconstruction, following previous work [39]. First, we optimize the coarse keypoint loss  $\mathcal{L}_{kp}$ , which consists of the  $\ell_1$  loss for both 3D and 2D joint positions:

$$\mathcal{L}_{kp} = \|\hat{\mathbf{J}}_{3d} - \mathbf{J}_{3d}\|_{1} + \|\hat{\mathbf{J}}_{2d} - \mathbf{J}_{2d}\|_{1}. \tag{1}$$

Since the proposed dataset 4DHuman-SKEL provides reliable parameter ground truth, we further impose parameter-level supervision for the shape  $\beta$  and pose  $\theta$ , which denotes as  $\mathcal{L}_{\beta}$  and  $\mathcal{L}_{\theta}$  respectively:

$$\mathcal{L}_{\beta} = \|\hat{\boldsymbol{\beta}} - \boldsymbol{\beta}\|_{1}, \, \mathcal{L}_{\theta} = \|\hat{\boldsymbol{\theta}} - \boldsymbol{\theta}\|_{1} \tag{2}$$

Finally, to learn target parameter  $\hat{\Theta} = \{\hat{\theta}, \hat{\beta}, \hat{\pi}\}$ , we use  $\mathcal{L}_{skel}$  which is a combination of the three losses:

$$\mathcal{L}_{\text{skel}} = \lambda_{kp} \mathcal{L}_{\text{kp}} + \lambda_{\beta} \mathcal{L}_{\beta} + \lambda_{\theta} \mathcal{L}_{\theta} \tag{3}$$

where  $\lambda_{kp}$ ,  $\lambda_{\beta}$  and  $\lambda_{\theta}$  are hyper-parameters.

Coarse-to-fine refinement. Accurately regressing pose and shape parameters in a single forward pass is challenging, especially for complex articulations such as yoga poses. To mitigate this, SKEL-CF adopts a coarse-to-fine refinement strategy. The encoder first produces an initial estimate of the parameters, denoted as  $\Theta_0 = \{\theta_0, \beta_0, \pi_0\}$ . The decoder then refines these predictions across L layers, where the i-th layer outputs  $\Theta_i = \{\theta_i, \beta_i, \pi_i\}$ . The final layer produces the refined prediction  $\Theta_L$ . Both the encoder output and the final decoder output are optimized using the same objective function  $\mathcal{L}_{\rm skel}$ :

$$\mathcal{L}_{enc} = \mathcal{L}_{skel}, \quad \mathcal{L}_{dec} = \mathcal{L}_{skel}.$$
 (4)

To stabilize training, each decoder layer is supervised individually. Specifically, the pose parameters predicted at each layer are optimized with the following refinement loss:

$$\mathcal{L}_{\text{refine}} = \sum_{i=1}^{L} \|\hat{\boldsymbol{\theta}}_i - \boldsymbol{\theta}_i\|_1, \tag{5}$$

where L denotes the total number of decoder layers.

**Overall optimization goal.** The overall loss function combines the above components for both the coarse encoder prediction and the refinement decoder:

$$\mathcal{L}_{tot} = \mathcal{L}_{dec} + \mathcal{L}_{enc} + \lambda_{ref} \mathcal{L}_{refine}, \tag{6}$$

where  $\lambda_{ref}$  is the coefficient for the refinement loss.

Implementation details. Following HSMR [39], we adopt ViTPose-H [41], pretrained on COCO [22], as the encoder backbone. ViTPose-H consists of 32 transformer layers, each with 16 attention heads and a hidden dimension of 1280. The decoder is a standard transformer decoder with L=6 layers, consistent with the design in HSMR [39]. We train SKEL-CF using the AdamW [24] optimizer with  $\beta_1$ ,  $\beta_2$  setting to 0.9, 0.999, weight decay setting to  $1\times 10^{-4}$ , a batch size of 64 and a learning rate of  $1\times 10^{-5}$ , preceded by a one-epoch warm-up. Training is conducted

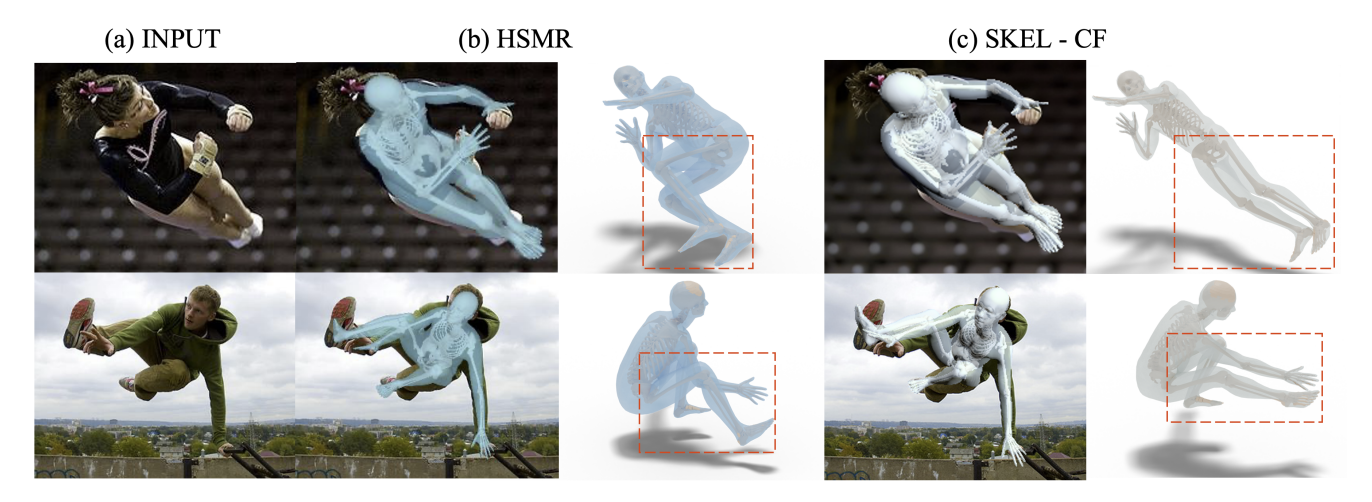


Figure 3. Visual comparison between the proposed SKEL-CF and HSMR [39]. Our proposed SKEL-CF achieves more precise skeletal estimations (best viewed in zoom). Additional visual results are provided in the supplementary material.

for 30 epochs on 8 NVIDIA A100 GPUs, taking approximately 120 hours in total. The hyper-parameters are set as  $\lambda_{kp}=0.05,\,\lambda_{\beta}=0.0005,\,\lambda_{\theta}=0.001,\,$  and  $\lambda_{ref}=0.1.$  Notably, our training schedule is significantly shorter than that of HSMR [39], which trains for 100 epochs.

## 4. Experiment

In this section, we first introduce the datasets and evaluation metrics in Section 4.1. We then provide a comparison between SKEL-based methods in Section 4.2 and SMPL-based approaches in Section 4.3. Finally, we present the ablation studies and additional discussions in Section 4.4.

## 4.1. Datasets and evaluation metrics

Evaluated datasets. We evaluate SKEL-CF on five representative datasets covering diverse environments and motion complexities, following standard practice [4, 11, 27, 39]. 3DPW [35] provides in-the-wild videos with accurate 3D annotations captured by moving cameras. Human3.6M [9] includes controlled indoor actions (e.g., sitting, walking, greeting) with motion-capture ground truth. EMDB [14] offers high-quality pose and shape sequences captured with electromagnetic sensors and handheld cameras. SPEC-SYN [17] is synthetic with explicit camera intrinsics and diverse perspectives for controlled camera evaluation. In contrast, MOYO [33] contains large-scale yoga sequences with extreme poses, frequent self-occlusions, and ground contact, providing the most challenging and diverse test scenario. Since most yoga videos in MOYO starts and ends with the same static poses, we select the front-view camera among the eight available viewpoints and remove the first and last 25% of frames to retain the complex and diverse motion segments, forming the curated MOYO-HARD subset. More details are provided in Appendix, Figure S5., where we additionally include visualizations of the removed first and last 25% segments of the MOYO videos.

**Evaluation metrics.** We evaluate the 3D human body recovery using MPJPE, PA-MPJPE, and PVE. Among them, MPJPE and PA-MPJPE serve as sparse evaluations, measuring the Euclidean distance between the predicted and ground-truth kinematic joints before and after rigid alignment, respectively. In contrast, PVE provides a dense evaluation, computing the vertex-level error between the predicted and ground-truth meshes, thereby offering a more comprehensive assessment of surface reconstruction accuracy. The 2D keypoint metrics, PCK@0.05 and PCK@0.1, which quantify the ratio of projected keypoints within a normalized distance threshold to the ground truth.

#### 4.2. Comparison with SKEL-based approaches.

Quantitative results. We compare to SKEL-based [15] approaches in Table 1. Our proposed SKEL-CF achieves consistent and significant improvements over both HSMR [39] and the optimization-based SKEL [15] baseline across all benchmarks. SKEL-CF achieces significant improvement compared to previous approach arcoss all the three datasets. Notably, on the challenging MOYO [33] dataset, which involves large pose variations, self-occlusion, and ground contact, posing substantial challenges for accurate pose and shape estimation. SKEL-CF shows a clear advantage in this setting, achieving up to 18.6% in terms of MPJPE and 35.4% improvement on PA-MPJPE.

**Visual results.** We provide a visual comparison with HSMR [39] in Figure 3. As shown, the proposed SKEL-CF achieves more accurate skeletal estimation and mesh re-

Method	3DPW [35]			EMDB [14]		SPEC-SYN [17]		MOYO [33]		MOYO-HARD					
	MPJPE↓	PA-MPJPE↓	PVE↓	MPJPE↓	PA-MPJPE↓	PVE↓	MPJPE↓	PA-MPJPE↓	PVE↓	MPJPE↓	PA-MPJPE↓	PVE↓	MPJPE↓	PA-MPJPE↓	PVE↓
SMPL [23]-based Approaches															
SPEC [17]	96.5	53.2	118.5	138.9	87.7	161.3	83.5	56.9	98.9	-	-	-	-	-	-
CLIFF [21]	69.0	43.0	81.2	103.5	68.3	123.7	128.5	55.8	139.0	154.6	109.3	155.7	-	-	-
HMR2.0a [6]	69.8	44.4	82.2	97.8	61.5	120.0	133.3	55.8	153.0	-	-	-	-	-	-
TokenHMR [4]	70.5	43.8	86.0	88.1	49.8	104.2	110.5	51.8	127.6	-	-	-	-	-	-
WHAM [30]	57.8	35.9	68.7	79.7	50.4	94.4	-	-	-	-	-	-	-	-	-
ReFit [36]	57.6	38.2	67.6	91.7	55.5	106.2	103.6	51.3	116.3	-	-	-	-	-	-
CLIFF [21]	72.0	46.6	85.0	97.1	61.3	113.2	109.9	55.6	124.6	-	-	-	-	-	-
HMR2.0b [6]	81.3	54.3	93.1	118.5	79.2	140.6	150.7	67.6	172.9	123.3	90.4	142.2	-	-	-
CameraHMR [27]	62.7	38.7	73.4	73.2	43.9	85.6	66.0	37.0	79.1	85.1	50.2	95.3	96.0	61.9	111.8
SKEL [15]-based Approaches															
HSMR [39]	81.5	54.8	-	-	-	-	-	-	-	104.5	79.6	120.1	120.0	97.7	140.5
SKEL-CF (Ours)	61.5	38.7	73.5	72.0	44.5	84.7	69.4	37.1	83.4	85.0	51.4	91.9	90.0	61.5	102.5

Table 2. Quantitative comparison of mesh recovery using the SMPL [23] human model on 3DPW [35], EMDB [14], SPEC-SYN [17], MOYO [33], and the more challenging MOYO-Hard dataset. The proposed SKEL-based method, SKEL-CF, achieves performance competitive with CameraHMR [27], with more pronounced improvements on complex motion scenarios as MOYO-Hard.

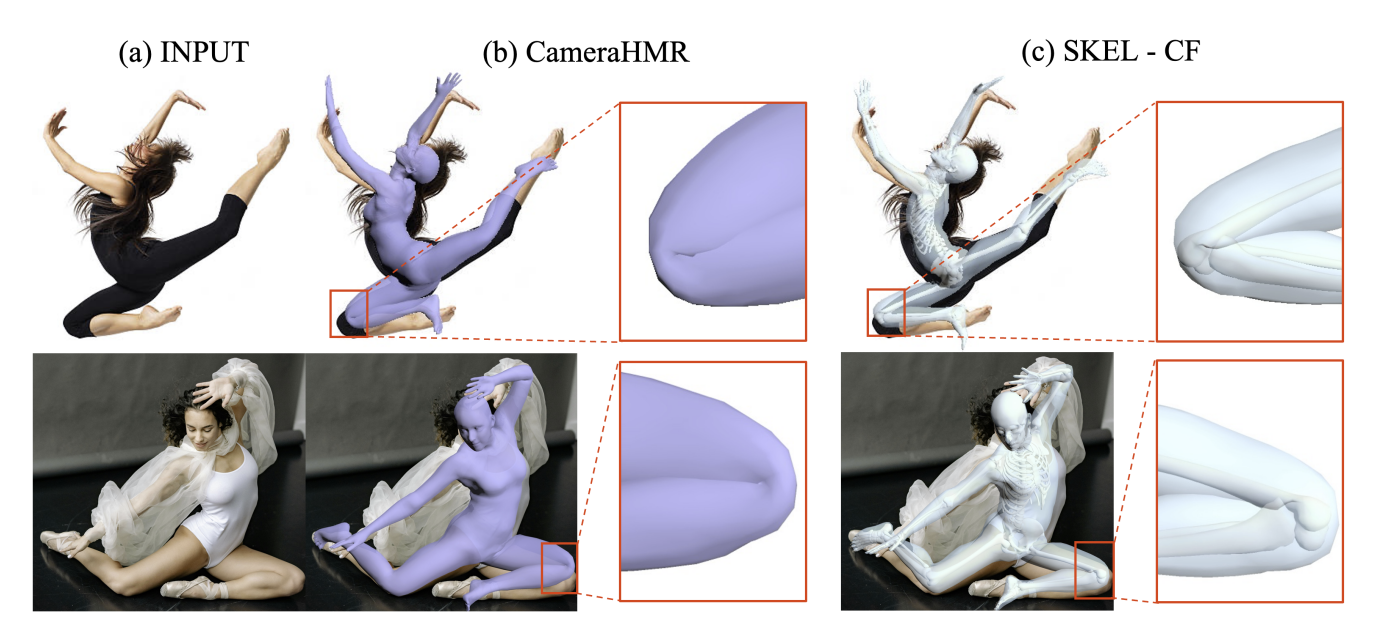


Figure 4. Visual comparison between the proposed SKEL-CF and CameraHMR [27]. The proposed SKEL-CF is built upon the SKEL [15] representation, which enforces anatomically consistent joint motion, resulting in more natural pose predictions compared to the SMPL [23]-based CameraHMR [27] (best viewed in zoom). Additional visual examples are provided in the supplementary material.

construction. More visual examples similar to Figure 3 are included in in Appendix, Figure S2.

### 4.3. Comparison with SMPL-based approaches

Quantitative results. We further compare SKEL-CF with recent state-of-the-art SMPL-based human mesh recovery methods across four representative datasets: 3DPW [35], EMDB [14], SPEC-SYN [17], MOYO [33] and more challenging MOYO-HARD, as summarized in Table 2. Note that SMPL [23] is less constrained compared to SKEL [15], enable achieving strong quantitative performance but occasionally producing anatomical inconsistency or unnatural joint motions(see Figure 1). Despite this inherent difference, SKEL-CF achieves comparable performance to Cam-

eraHMR [27], the strongest SMPL-based model trained on 4DHuman, demonstrating that kinematically constrained SKEL representations can reach a similar level of numerical precision while maintaining stronger physical plausibility.

Notably, on the challenging MOYO [33] dataset, which contains complex yoga sequences with strong self-occlusion and body-ground interactions, SKEL-CF achieves state-of-the-art performance in dense mesh prediction (PVE) and overall reconstruction accuracy. Furthermore, on the MOYO-HARD subset, focused on dynamic and highly articulated poses, SKEL-CF consistently outperforms all SMPL-based baselines across all metrics (MPJPE, PA-MPJPE, and PVE). This highlights its superior ability to maintain accurate and physically realistic motion represen-



Figure 5. **Illustration of the mesh refinement process.** The light green meshes represent the initial coarse estimations, while the dark green meshes denote the progressively refined final results.

tations under extreme articulations. These results demonstrate that SKEL-CF provides a scalable and anatomically faithful framework for human motion analysis, bridging the gap between computer vision and biomechanics. For completeness, we also report the 2D keypoint results in Table 3. Our approach achieves comparable accuracy under PCK@0.1, indicating that the projected mesh provides a consistent and accurate fit to the 2D image plane.

**Visual results.** We provide a visual comparison with the SMPL [23]-based state-of-the-art method CameraHMR [27] in Figure 4. As shown, the proposed SKEL-CF produces anatomically more consistent joint motions, benefiting from the structural constraints of the SKEL [15] model. In contrast, CameraHMR tends to generate unnatural joint configurations under complex motion scenarios. Additional visualizations similar to Figure 4 are provided in Appendix, Figure S1.

#### 4.4. Discussion

Ablation study. To analyze the contribution of each component, we conduct an ablation study on the MOYO [33] and COCO [22] datasets, representing 3D and 2D evaluation metrics, respectively. We progressively activate three key components: the camera model, the coarse-to-fine strategy, and the refinement stage, then report the corresponding performance under both 3D and 2D metrics. Incorporating the camera model notably improves the 3D reconstruction accuracy. The coarse-to-fine strategy further enhances the

Method	PCK@0.05↑	PCK@0.1↑
PyMAF [42]	0.68	0.86
CLIFF [21]	0.64	0.88
PARE [16]	0.72	0.91
PyMAF-X [43]	0.79	0.93
HMR2.0a [6]	0.79	0.94
CameraHMR [27]	0.84	0.94
HSMR [39]	0.85	0.96
SKEL-CF (Ours)	0.80	0.93

Table 3. **2D Keypoint Performance on COCO** [22]. For completeness, we also report PCK scores of the projected keypoints at thresholds of 0.05 and 0.1, showing that SKEL-CF achieves comparable 2D keypoint quality while maintaining significant better biomechanical mesh quality.

C	ompon	ents		MOYO [33]	COCO [22]			
Cam	C2F	Refine	MPJPE↓	PA-MPJPE↓	PVE↓	PCK@0.05↑	PCK@0.1↑	
×	Х	Х	88.8	53.7	97.0	0.76	0.91	
Х	/	/	89.5	54.8	97.9	0.79	0.93	
/	X	/	84.7	50.6	91.7	0.67	0.91	
/	1	Х	86.2	52.1	93.5	0.77	0.92	
<b>✓</b>	/	1	85.0	51.4	91.9	0.80	0.93	

Table 4. **Ablation study on MOYO** [33] and COCO [22]. *Cam* denotes the camera model, *C2F* represents the coarse-to-fine strategy, and *Refine* indicates the progressive refinement stage.

2D metrics. Finally, the refinement stage brings consistent improvements across both 3D and 2D evaluations.

**Iterative mesh refinement process.** We further visualize the iterative mesh refinement process of SKEL-CF in Figure 5. As shown, our model begins with a coarse estimation of the motion and progressively refines it through successive iterations, leading to a more accurate reconstruction of complex motions. This visualization clearly demonstrates the effectiveness of the proposed coarse-to-fine refinement strategy. Additional video results illustrating the refinement process are provided in the supplementary material.

### 5. Conclusion

In this work, we introduced SKEL-CF, a comprehensive biomechanical skeleton and surface mesh recovery pipeline built upon the SKEL representation. By transforming the high-quality SMPL dataset into a SKEL-based format, termed 4DHuman-SKEL, we established a strong foundation for accurate and generalizable training. Our integration of an explicit camera model effectively mitigates the limitations of weak-perspective assumptions seen in previous works such as HSMR, enabling robust pose estimation under diverse viewpoints. Furthermore, the proposed coarse-to-fine refinement strategy enables stable and high-fidelity reconstruction results. Overall, SKEL-CF sets a new baseline for biomechanical skeleton and surface recovery, providing a practical and extensible framework for future research in human modeling and motion understanding.

#### References

- [1] Mykhaylo Andriluka, Leonid Pishchulin, Peter Gehler, and Bernt Schiele. 2d human pose estimation: New benchmark and state of the art analysis. In *CVPR*, 2014. 4
- [2] Federica Bogo, Angjoo Kanazawa, Christoph Lassner, Peter Gehler, Javier Romero, and Michael J Black. Keep it smpl: Automatic estimation of 3d human pose and shape from a single image. In ECCV, 2016. 3
- [3] Nicolas Carion, Francisco Massa, Gabriel Synnaeve, Nicolas Usunier, Alexander Kirillov, and Sergey Zagoruyko. End-toend object detection with transformers. In ECCV, 2020. 4
- [4] Sai Kumar Dwivedi, Yu Sun, Priyanka Patel, Yao Feng, and Michael J Black. Tokenhmr: Advancing human mesh recovery with a tokenized pose representation. In CVPR, 2024. 3, 6, 7
- [5] Zipeng Fu, Qingqing Zhao, Qi Wu, Gordon Wetzstein, and Chelsea Finn. Humanplus: Humanoid shadowing and imitation from humans. In *CoRL*, 2024. 2
- [6] Shubham Goel, Georgios Pavlakos, Jathushan Rajasegaran, Angjoo Kanazawa, and Jitendra Malik. Humans in 4D: Reconstructing and tracking humans with transformers. In ICCV, 2023. 2, 3, 4, 7, 8
- [7] Chunhui Gu, Chen Sun, David A Ross, Carl Vondrick, Caroline Pantofaru, Yeqing Li, Sudheendra Vijayanarasimhan, George Toderici, Susanna Ricco, Rahul Sukthankar, et al. Ava: A video dataset of spatio-temporally localized atomic visual actions. In CVPR, 2018. 4
- [8] Tairan He, Zhengyi Luo, Wenli Xiao, Chong Zhang, Kris Kitani, Changliu Liu, and Guanya Shi. Learning humanto-humanoid real-time whole-body teleoperation. In *IROS*, 2024. 2
- [9] Catalin Ionescu, Dragos Papava, Vlad Olaru, and Cristian Sminchisescu. Human3. 6m: Large scale datasets and predictive methods for 3d human sensing in natural environments. *TPAMI*, 2013. 4, 5, 6
- [10] Sam Johnson and Mark Everingham. Learning effective human pose estimation from inaccurate annotation. In CVPR, 2011. 1, 4
- [11] Angjoo Kanazawa, Michael J Black, David W Jacobs, and Jitendra Malik. End-to-end recovery of human shape and pose. In CVPR, 2018. 3, 6
- [12] Angjoo Kanazawa, Jason Y Zhang, Panna Felsen, and Jitendra Malik. Learning 3d human dynamics from video. In CVPR, 2019. 4
- [13] Angjoo Kanazawa, Jason Y Zhang, Panna Felsen, and Jitendra Malik. Learning 3d human dynamics from video. In CVPR, 2019. 4
- [14] Manuel Kaufmann, Jie Song, Chen Guo, Kaiyue Shen, Tianjian Jiang, Chengcheng Tang, Juan José Zárate, and Otmar Hilliges. EMDB: The Electromagnetic Database of Global 3D Human Pose and Shape in the Wild. In *ICCV*, 2023. 2, 6. 7
- [15] Marilyn Keller, Keenon Werling, Soyong Shin, Scott Delp, Sergi Pujades, C Karen Liu, and Michael J Black. From skin

- to skeleton: Towards biomechanically accurate 3d digital humans. *TOG*, 2023. 2, 4, 5, 6, 7, 8, 1, 3
- [16] Muhammed Kocabas, Chun-Hao P Huang, Otmar Hilliges, and Michael J Black. PARE: Part attention regressor for 3D human body estimation. In *ICCV*, 2021. 8
- [17] Muhammed Kocabas, Chun-Hao P. Huang, Joachim Tesch, Lea Müller, Otmar Hilliges, and Michael J. Black. SPEC: Seeing people in the wild with an estimated camera. In *ICCV*, 2021. 6, 7
- [18] Nikos Kolotouros, Georgios Pavlakos, Dinesh Jayaraman, and Kostas Daniilidis. Probabilistic modeling for human mesh recovery. In *ICCV*, 2021. 3, 4
- [19] Jinhan Li, Yifeng Zhu, Yuqi Xie, Zhenyu Jiang, Mingyo Seo, Georgios Pavlakos, and Yuke Zhu. Okami: Teaching humanoid robots manipulation skills through single video imitation. In CoRL, 2024. 2
- [20] Tianye Li, Timo Bolkart, Michael J Black, Hao Li, and Javier Romero. Learning a model of facial shape and expression from 4d scans. *ACM Trans. Graph.*, 2017. 2
- [21] Zhihao Li, Jianzhuang Liu, Zhensong Zhang, Songcen Xu, and Youliang Yan. Cliff: Carrying location information in full frames into human pose and shape estimation. In ECCV, 2022. 3, 7, 8
- [22] Tsung-Yi Lin, Michael Maire, Serge Belongie, James Hays, Pietro Perona, Deva Ramanan, Piotr Dollár, and C Lawrence Zitnick. Microsoft coco: Common objects in context. In ECCV, 2014. 4, 5, 8
- [23] Matthew Loper, Naureen Mahmood, Javier Romero, Gerard Pons-Moll, and Michael J Black. Smpl. TOG, 2015. 2, 3, 4, 7, 8, 1
- [24] Ilya Loshchilov and Frank Hutter. Decoupled weight decay regularization. In *ICLR*, 2017. 5
- [25] Naureen Mahmood, Nima Ghorbani, Nikolaus F Troje, Gerard Pons-Moll, and Michael J Black. Amass: Archive of motion capture as surface shapes. In *ICCV*, 2019. 3
- [26] Dushyant Mehta, Helge Rhodin, Dan Casas, Pascal Fua, Oleksandr Sotnychenko, Weipeng Xu, and Christian Theobalt. Monocular 3d human pose estimation in the wild using improved CNN supervision. In 3DV, 2017. 4
- [27] Priyanka Patel and Michael J Black. Camerahmr: Aligning people with perspective. In *3DV*, 2025. 1, 2, 3, 4, 6, 7, 8
- [28] Georgios Pavlakos, Vasileios Choutas, Nima Ghorbani, Timo Bolkart, Ahmed AA Osman, Dimitrios Tzionas, and Michael J Black. Expressive body capture: 3d hands, face, and body from a single image. In CVPR, 2019. 2
- [29] Javier Romero, Dimitrios Tzionas, and Michael J Black. Embodied hands: modeling and capturing hands and bodies together. *TOG*, 2017. 2
- [30] Soyong Shin, Juyong Kim, Eni Halilaj, and Michael J Black. Wham: Reconstructing world-grounded humans with accurate 3d motion. In CVPR, 2024. 7
- [31] Yu Sun, Yun Ye, Wu Liu, Wenpeng Gao, Yili Fu, and Tao Mei. Human mesh recovery from monocular images via a skeleton-disentangled representation. In *ICCV*, 2019. 4
- [32] Guy Tevet, Sigal Raab, Brian Gordon, Yoni Shafir, Daniel Cohen-or, and Amit Haim Bermano. Human motion diffusion model. In *ICLR*, 2022. 2

- [33] Shashank Tripathi, Lea Müller, Chun-Hao P Huang, Omid Taheri, Michael J Black, and Dimitrios Tzionas. 3d human pose estimation via intuitive physics. In *CVPR*, 2023. 2, 3, 5, 6, 7, 8, 1
- [34] Aaron Van Den Oord, Oriol Vinyals, et al. Neural discrete representation learning. *NeurIPS*, 2017.
- [35] Timo Von Marcard, Roberto Henschel, Michael J Black, Bodo Rosenhahn, and Gerard Pons-Moll. Recovering accurate 3d human pose in the wild using imus and a moving camera. In ECCV, 2018. 2, 5, 6, 7
- [36] Yufu Wang and Kostas Daniilidis. Refit: Recurrent fitting network for 3d human recovery. In *ICCV*, 2023. 7
- [37] Chung-Yi Weng, Brian Curless, Pratul P Srinivasan, Jonathan T Barron, and Ira Kemelmacher-Shlizerman. Humannerf: Free-viewpoint rendering of moving people from monocular video. In *CVPR*, 2022. 2
- [38] Jiahong Wu, He Zheng, Bo Zhao, Yixin Li, Baoming Yan, Rui Liang, Wenjia Wang, Shipei Zhou, Guosen Lin, Yanwei Fu, et al. Ai challenger: A large-scale dataset for going deeper in image understanding. *arXiv*, 2017. 4
- [39] Yan Xia, Xiaowei Zhou, Etienne Vouga, Qixing Huang, and Georgios Pavlakos. Reconstructing humans with a biomechanically accurate skeleton. In CVPR, 2025. 1, 2, 4, 5, 6, 7, 8, 3
- [40] Hongyi Xu, Eduard Gabriel Bazavan, Andrei Zanfir, William T Freeman, Rahul Sukthankar, and Cristian Sminchisescu. Ghum & ghuml: Generative 3d human shape and articulated pose models. In CVPR, 2020. 2
- [41] Yufei Xu, Jing Zhang, Qiming Zhang, and Dacheng Tao. ViTPose: Simple vision transformer baselines for human pose estimation. In *NeurIPS*, 2022. 5
- [42] Hongwen Zhang, Yating Tian, Xinchi Zhou, Wanli Ouyang, Yebin Liu, Limin Wang, and Zhenan Sun. Pymaf: 3d human pose and shape regression with pyramidal mesh alignment feedback loop. In *ICCV*, 2021. 8
- [43] Hongwen Zhang, Yating Tian, Yuxiang Zhang, Mengcheng Li, Liang An, Zhenan Sun, and Yebin Liu. Pymaf-x: Towards well-aligned full-body model regression from monocular images. *TPAMI*, 2023. 8

# SKEL-CF: Coarse-to-Fine Biomechanical Skeleton and Surface Mesh Recovery

# Supplementary Material

## S1. Organization

This supplementary document is organized as follows:

- This supplementary material includes additional video demonstrations showcasing both our SKEL-CF visualizations and comparative results with HSMR [39] and CameraHMR [27] (located in the videos-demo folder). It also provides extended coarse-to-fine visualizations (in the coarse-to-fine-gif folder) and the supplementary PDF (SKEL-CF-sup.pdf).
- Additional qualitative results comparing our method with the SKEL-based model HSMR [39] are presented in Fig. S2.
- Additional qualitative comparisons with the SMPL [23]based approach CameraHMR [27] are provided in Fig S1.
- Details on the MOYO-HARD subset are in Section S6, see line 380 of the main text.
- More visual results illustrating our coarse-to-fine refinement strategy are shown in Fig. S3, as a supplement to Fig. 5 in the main text (line 468).
- Section \$5 analyzes the per-layer attention behavior of Pose, Beta, and Cam tokens.

#### S2. Visual comparison with SMPLs

To more comprehensively evaluate our model, we present in Fig. S1 additional visual comparisons extending the results shown in Fig. 4 of the main paper. These examples further compare our method with the state-of-the-art SMPL [23]-based approach, CameraHMR [27]. It indicates that our method can reconstruct more natural pose with accurate anatomical joints.

## S3. Visual comparison with SKELs

To further compare SKEL [15]-based approaches, Fig. S2 shows additional qualitative comparisons with the state-of-the-art HSMR [39] pipeline. Unlike HSMR, our method incorporates explicit camera modeling, enabling more reliable and accurate pose reconstruction under varying viewpoints.

#### S4. More results of Coarse-to-Fine

Figure S3 presents additional visual examples from LSP-ext [10], highlighting how the refinement process progressively improves pose and shape estimation.

Table S1. **COCO results under different camera extrinsic factorizations**  $(s, t_x, t_y)$ . (A) Fix final SKEL [15] parameters and s, vary layer-wise  $(t_x, t_y)$ . (B) Fix final SKEL parameters and  $(t_x, t_y)$ , vary layer-wise s.

Layer $\mid$ (A) Final Pose + $s$ ; Layer $(t_x, t_y) \mid$ (B) Final Pose + $(t_x, t_y)$ ; Layer $s$								
	PCK@0.05	PCK@0.1	PCK@0.05	PCK@0.1				
0	0.1147	0.4156	0.0164	0.0597				
1	0.0462	0.2493	0.0171	0.0604				
2	0.0312	0.1876	0.0193	0.0669				
3	0.1205	0.6088	0.0290	0.1038				
4	0.5592	0.8837	0.0689	0.2643				
5	0.8037	0.9361	0.8037	0.9360				

## **S5. Per-Layer Attention Analysis**

Figure S4 visualizes the attention regions of the Pose, Beta, and Cam tokens across different decoder layers. In Figure \$4(a), we show representative examples of the final Pose, Beta, and Cam tokens. We observe that the Pose token primarily attends to the interior body regions, the Beta token focuses on the body silhouette, and the Cam token concentrates on the surrounding environment, as it must aggregate contextual information to estimate the camera extrinsics. In Figure \$4(b)-(c), we visualize layer-wise attention for the same sample. The Pose token gradually shifts across different body parts, the Beta token evolves from the head region to the full silhouette, and the Cam token expands from the human region to the environment for estimating camera extrinsics. As shown in Table \$1, our ablation further reveals that layers 1–5 mainly learn 2D translation, while the final layer predominantly captures scale (depth).

# S6. Details of MOYO-HARD dataset

The MOYO [33] test set consists of 29 yoga sequences, each recorded simultaneously by eight cameras capturing the same pose from different viewpoints. Each sequence progresses from simple poses to complex ones and then returns to simpler poses, as shown in Figure S5. To specifically analyze performance under challenging poses, we focus on the middle portion of each sequence, where the motions are most complex. Accordingly, we construct the MOYO-HARD subset by selecting the middle 50% of frames from videos captured by Camera #1 (front view), resulting in a total of 9,725 images.

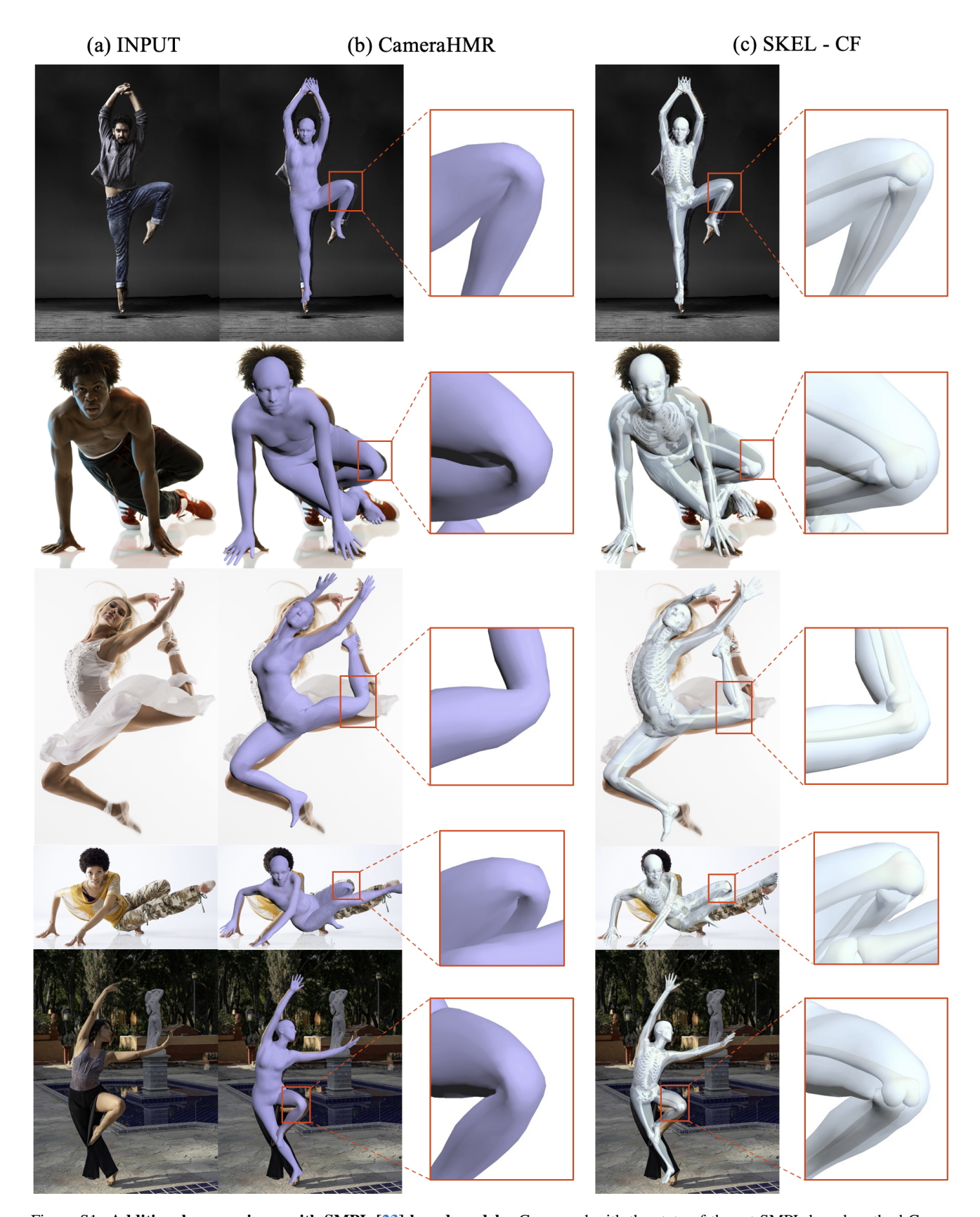


Figure S1. Additional comparisons with SMPL [23]-based models. Compared with the state-of-the-art SMPL-based method CameraHMR [27], our approach produces more natural and anatomically consistent joint predictions.

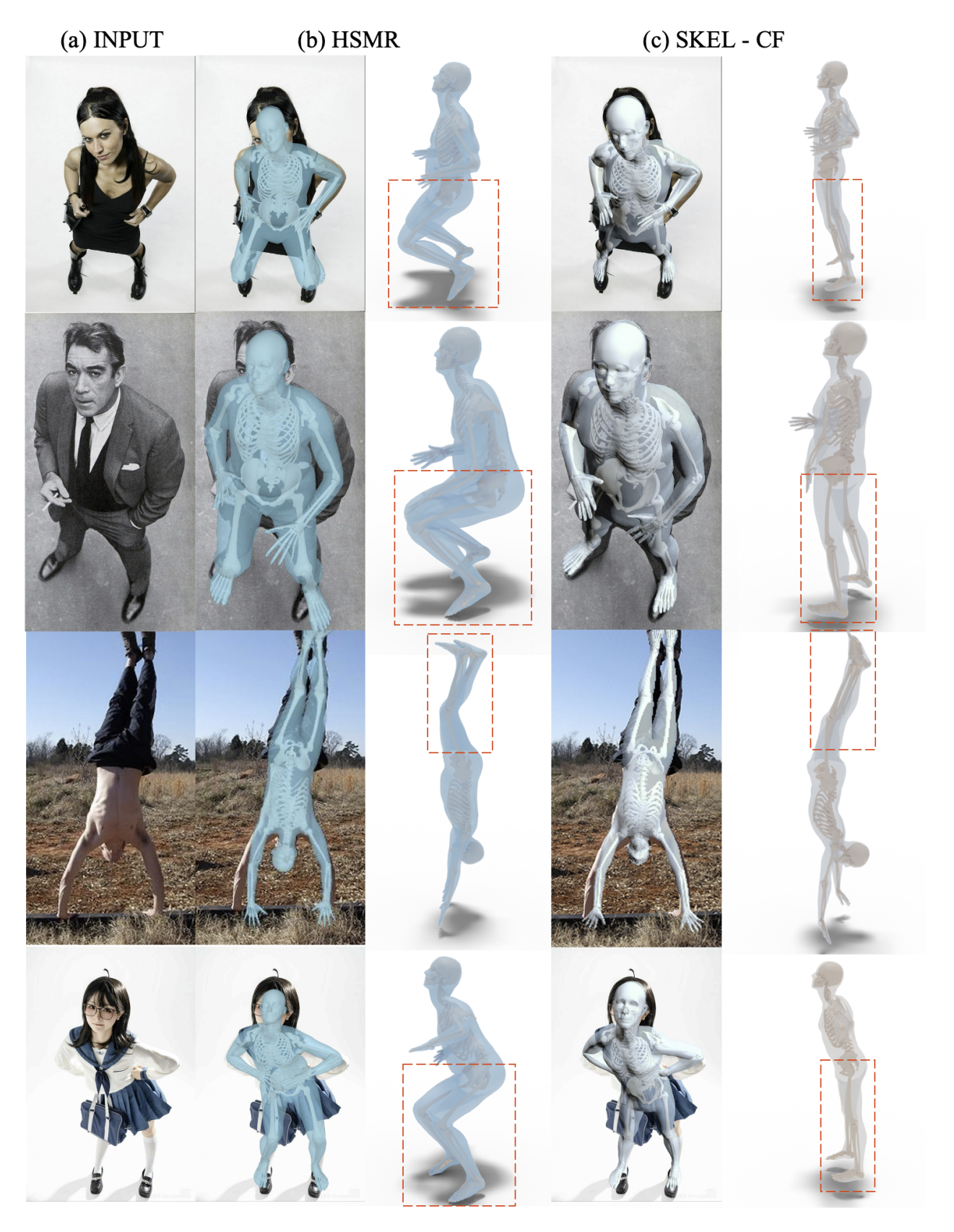


Figure S2. Additional comparisons with SKEL [15]-based models. Compared with the state-of-the-art HSMR [39] method, our approach predicts human poses that are more realistic and accurate.

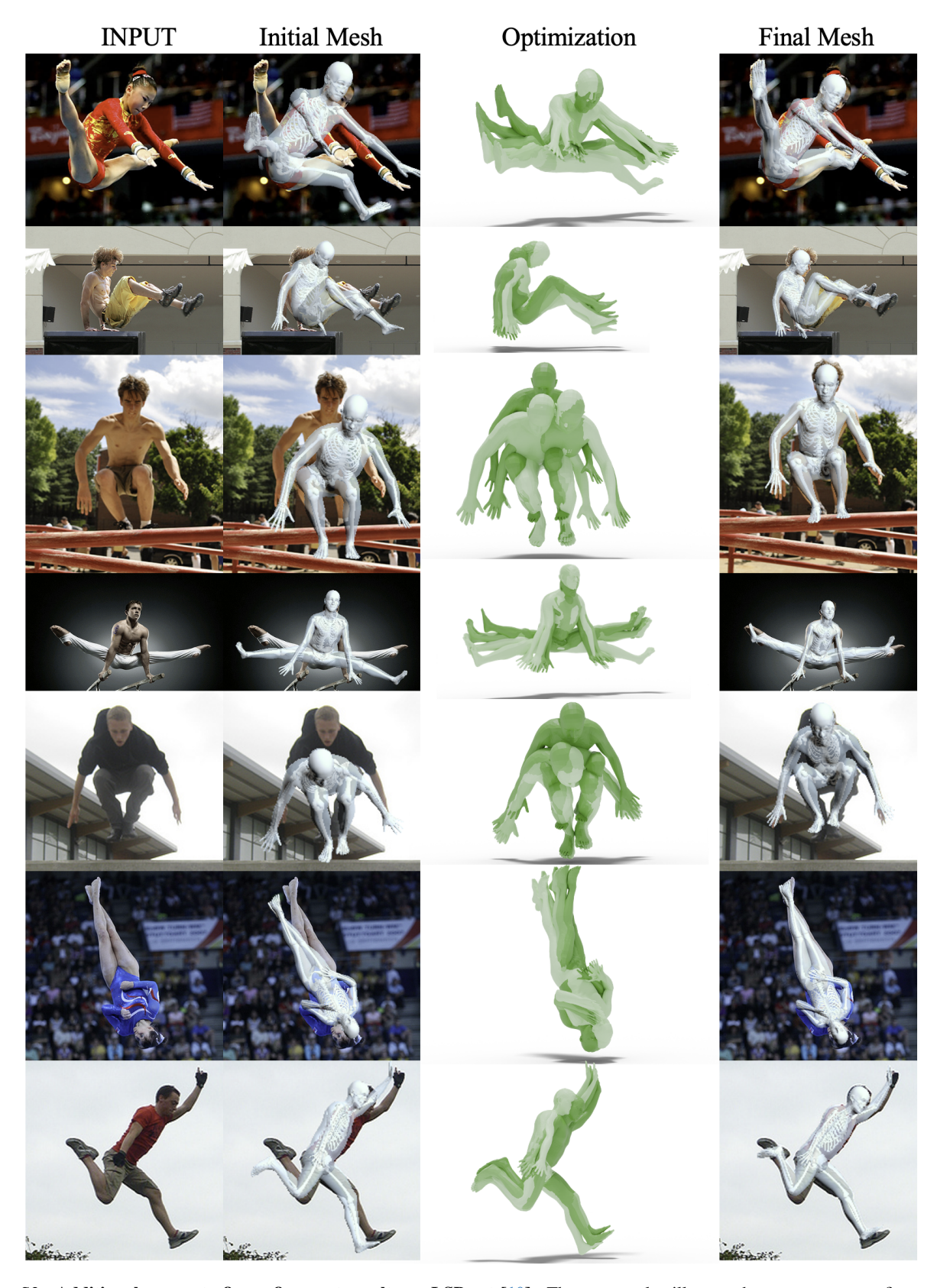


Figure S3. Additional coarse-to-fine refinement results on LSP-ext [10]. These examples illustrate how our coarse-to-fine strategy progressively improves pose and shape estimation, yielding more accurate and stable reconstructions across diverse human poses.

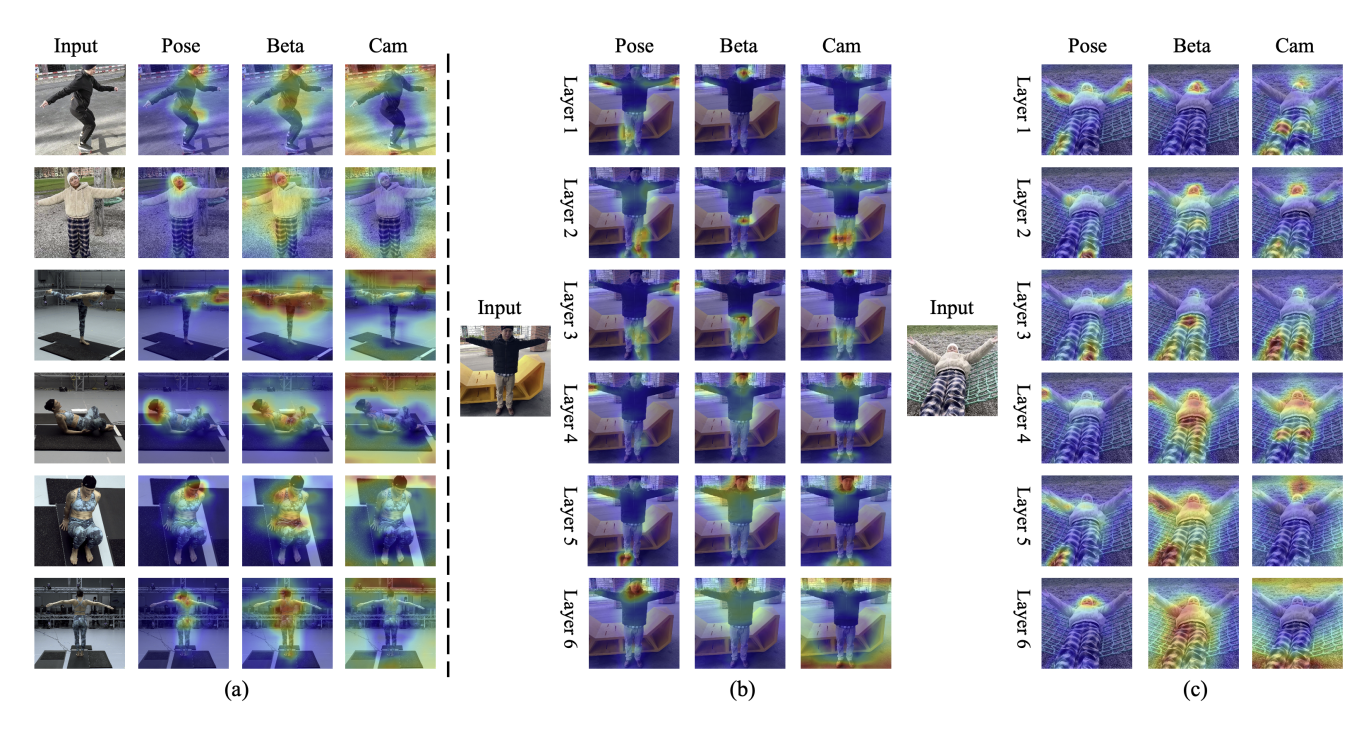


Figure S4. Layer-wise attention analysis of Pose, Beta, and Cam tokens. The Pose token progressively shifts across body parts, the Beta token expands from head to full silhouette, and the Cam token gradually incorporates scene context for estimating camera extrinsics.

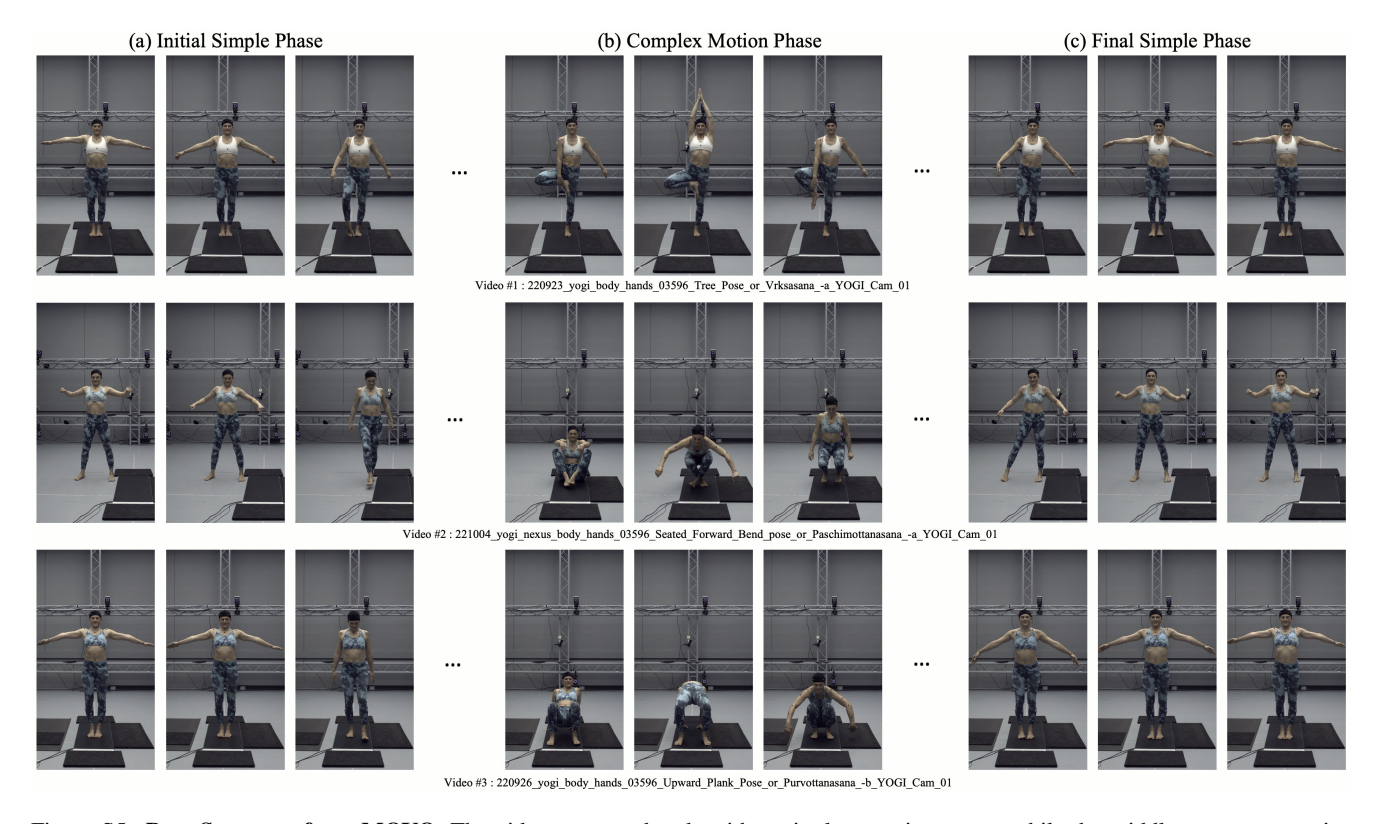


Figure S5. **Pose Sequence from MOYO.** The video starts and ends with static, low-motion poses, while the middle segment contains diverse, high-complexity movements, reflecting the overall difficulty distribution of the dataset.